Electronic Supplementary Material (ESI) for RSC Advances.

Supplementary Information

Melt processability and thermomechanical properties of blends based on polyhydroxyalkanoates and poly(butylene adipate-*co*-terephthalate)

Matilda Larsson[1,2], Olivia Markbo[1], Patric Jannasch[1]*

[1]Polymer & Materials Chemistry, Department of Chemistry, Lund University,
P.O. Box 124, SE-221 00, Lund, Sweden.
[2]Baxter Healthcare, Material and Platform, Magistratsvägen 16, SE-224 41, Lund, Sweden

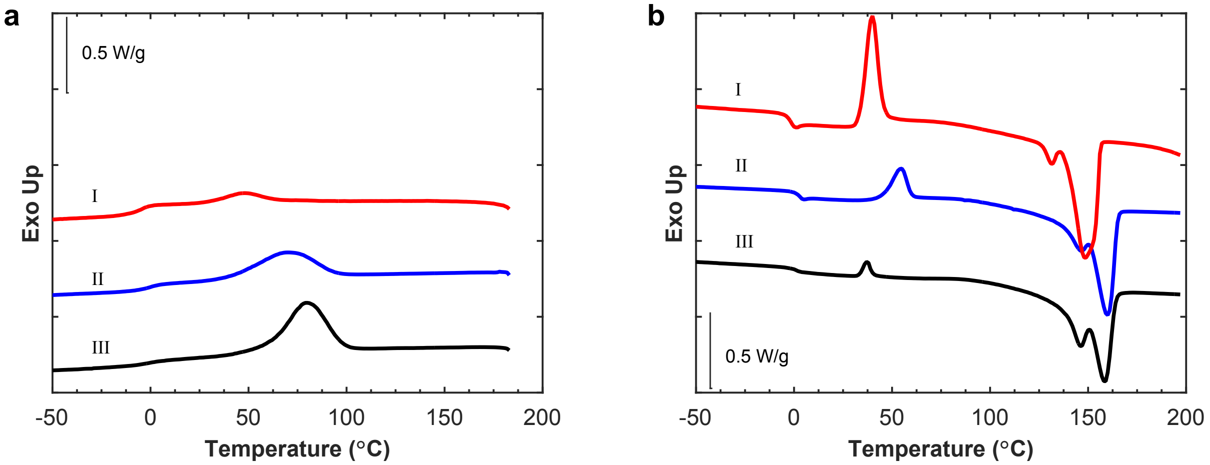

Figure S1: DSC traces of P(3,4HB) after different pre-treatments, (a) cooling and (b) second heating scans. [(I): as-received P(3,4HB), (II): after soxhlet extraction, (III): after aq. HCl-treatment]. The crystallization temperature, as well as the degree of crystallization, increased for the pre-treated samples. However, the cold crystallization decreased and the melting temperature increased after pre-treatment, indicating that the polymer crystallized more efficiently after the pre-treatment.

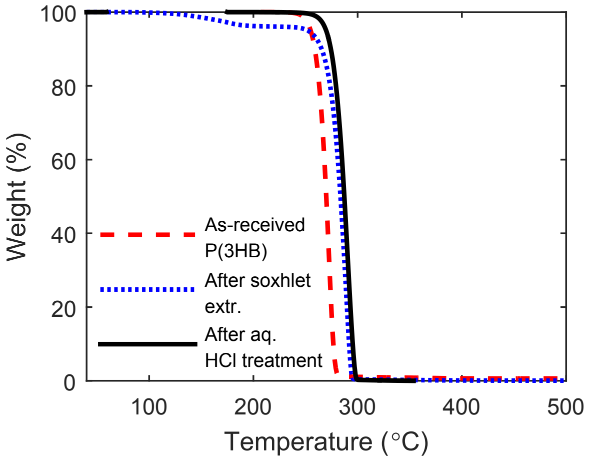

Figure S2: TGA traces of P(3HB) after different pre-treatments recorded at 10 °C/min under nitrogen. The decomposition temperatures increased by ~10 °C after the pre-treatments, compared to the as-received P(3HB).

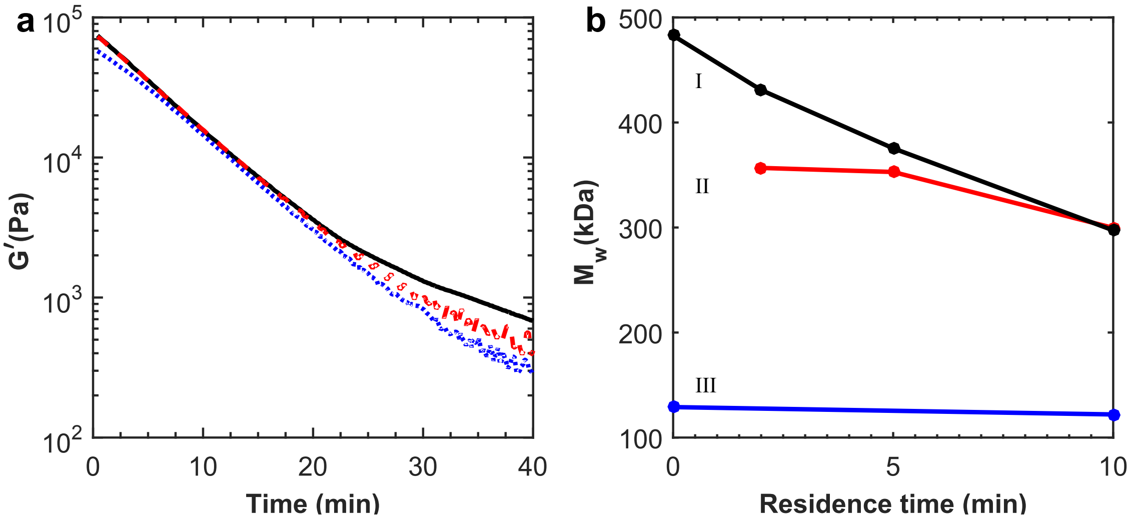

Figure S3: Shear storage modulus (a) and weight average molecular weights (b) of aq. HCl-treated (I) and as-received P(3HB) (II), and PBAT (III). It was not possible to analyze the as-received P(3HB) before extrusion. However, assuming the M_w to be identical to the aq. HCl-treated polymer [as observed for P(3,4HB)] there was a 40% decrease in M_w for the non-treated sample during the first 2 min. The M_w of the acid- treated sample decreased with 11% during the first 2 min. PBAT is also displayed for reference and shows a stable M_w value during 10 min.

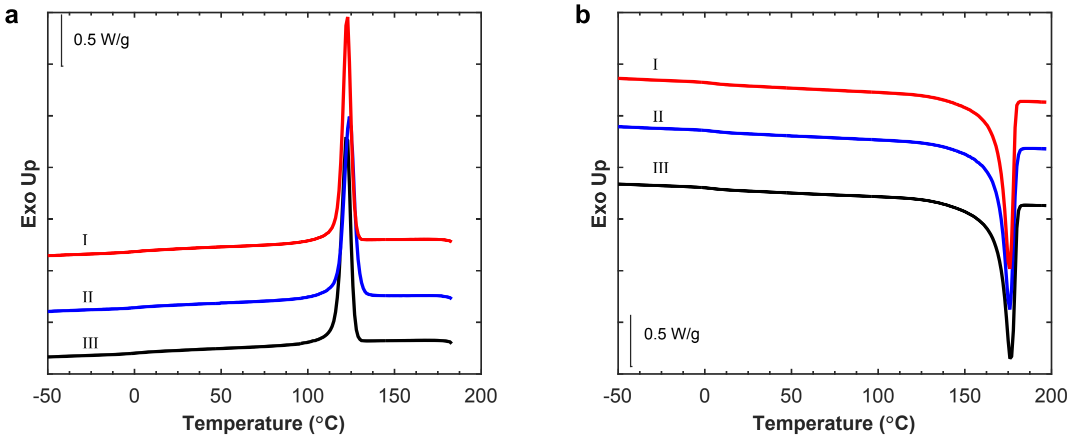

Figure S4: DSC traces of P(3HB) after different pre-treatments, (a) cooling and (b) second heating scans at 10 °C/min. [(I): as-received P(3,4HB), (II): after soxhlet extraction, (III): after aq. HCl-treatment]. Any effects of the pre-treatments were not noticeable in these measurements.

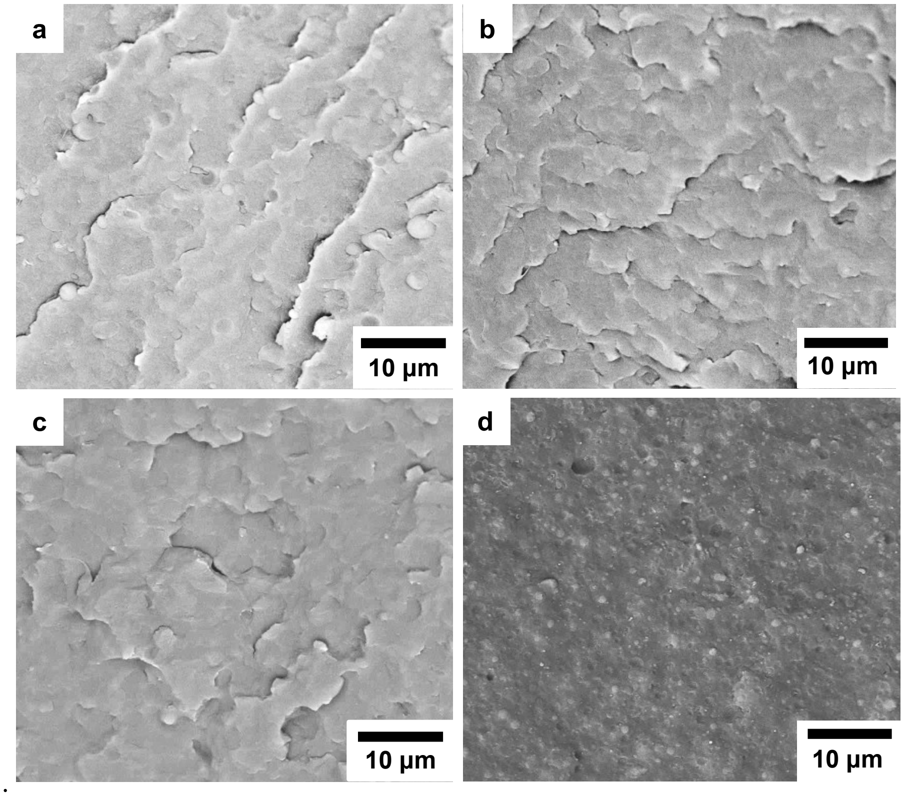

Figure S5: SEM images of cryo-fracture surfaces of P(3,4HB):PBAT blends with weight ratios (a) 20:80, (b) 40:60, (c) 60:40 and (d) 80:20. The phase separation was clearly visible for 80:20 blend with PBAT domains of approx. 1 µm in a matrix of P(3,4HB).

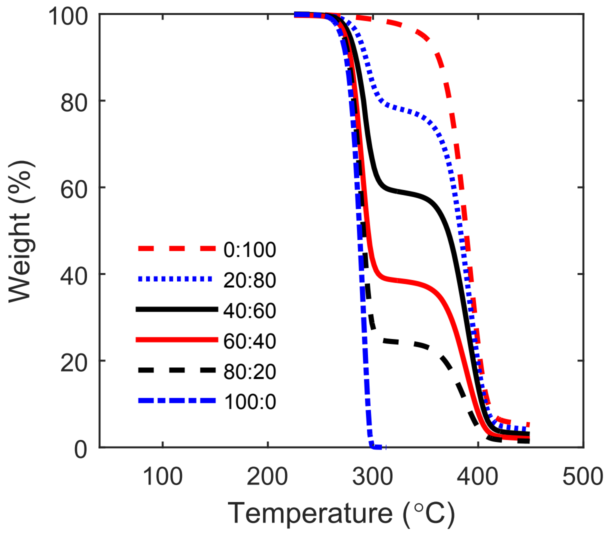

Figure S6: TGA traces of the P(3HB):PBAT blends.

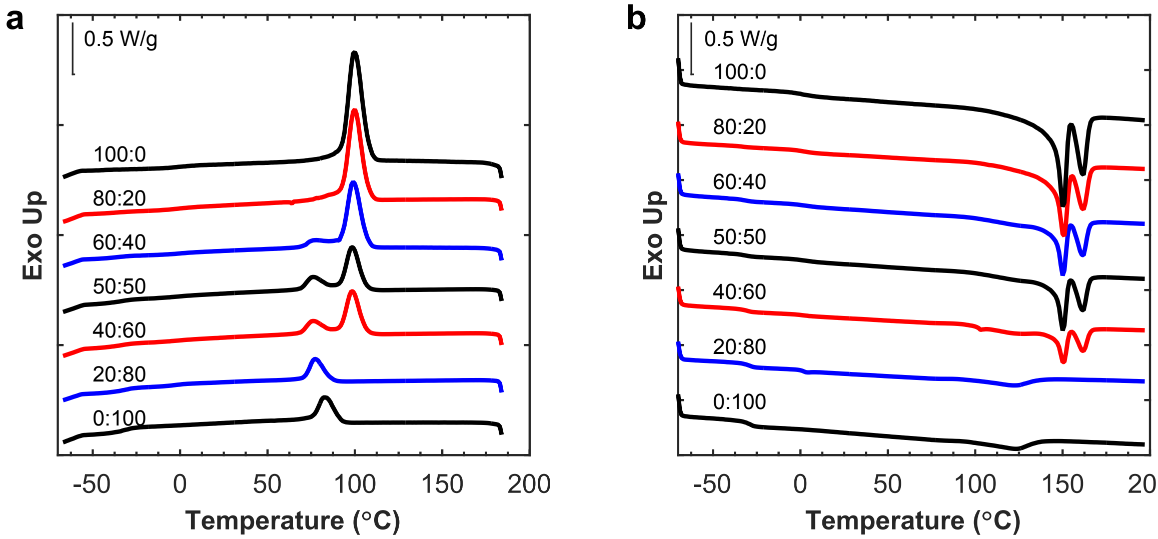

Figure S7: DSC traces of P(3,4HB):PBAT blends, (a) cooling and (b) second heating scans at 10 °C/min.

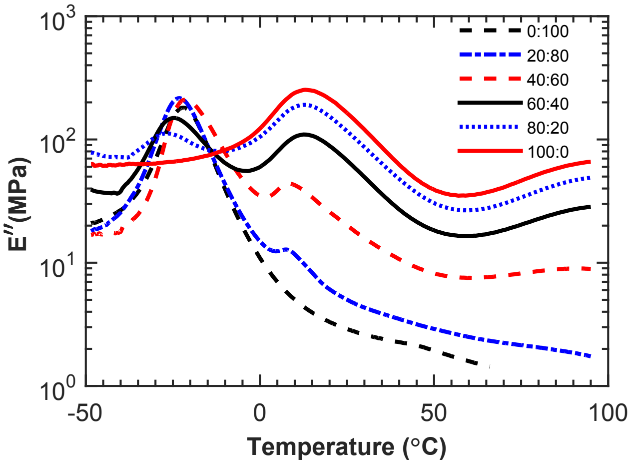

Figure S8: Tensile loss modulus measured by DMA of P(3HB):PBAT blends.

Table S1: Thermal properties of P(3,4HB):PBAT blends.

P(3,4HB):PBAT wt:wt	T_d^{PHA}/T_d^{PBAT} (°C)	$T_{m1}^{PHA}/T_{m1}^{PBAT}$ (°C)	$T_{m2}^{PHA}/T_{m2}^{PBAT}$ (°C)	T_c^{PHA}/T_c^{PBAT} (°C)
100:0	290/-	153/-	167/-	100/-
80:20	287/386	151/-	161/-	100/-
60:40	288/387	150/-	161/-	99/77
50:50	292/390	150/-	162/-	99/76
40:60	290/388	150/127	162/-	98/75
20:80	295/395	-/122	-/-	-/77
0:100	-/391	-/123	-/-	-/82

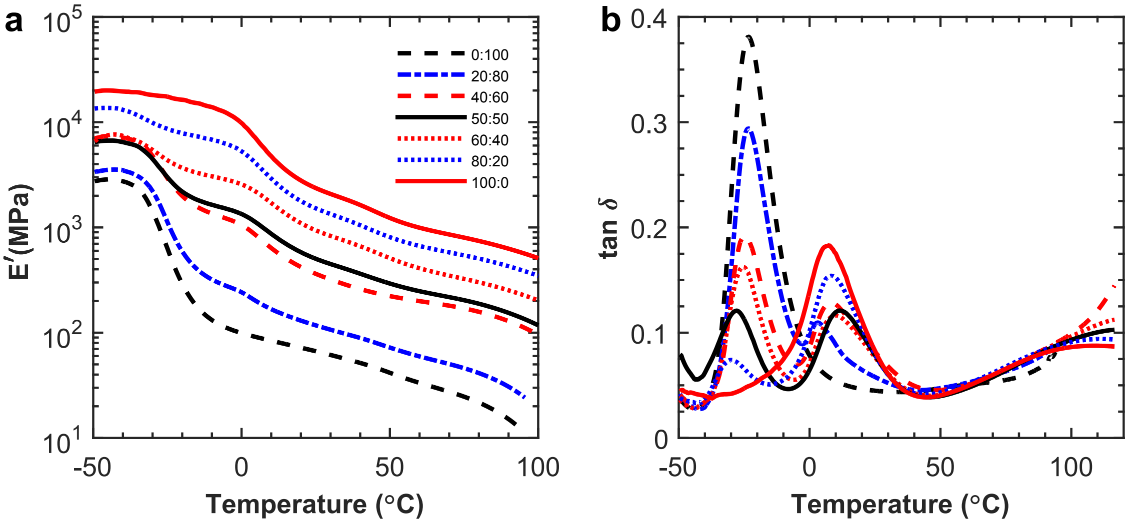

Figure S9: Tensile storage modulus (a) and tan δ curves (b) for P(3,4HB):PBAT blends, analyzed at 3 °C/min and 1 Hz in the linear viscoelastic. The storage modulus decreased with addition of PBAT with the largest decrease between 20 and 40 wt% PBAT indicating a phase inversion. Two visible tan δ peaks indicated the immiscibility of the blends.

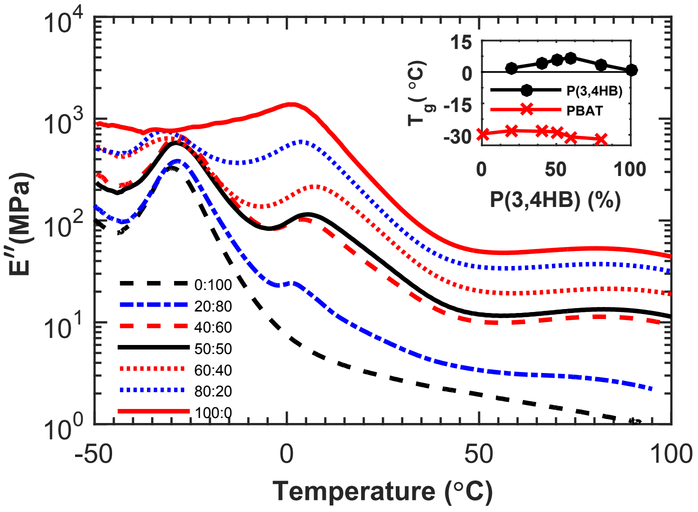

Figure S10: Tensile loss modulus measured by DMA of P(3,4HB):PBAT blends (a), and the T_g of P(3,4HB):PBAT blends determined from loss modulus peak value (b). The T_g for P(3,4HB) determined from the peak value of the loss modulus showed a maximum value at 60 wt% P(3,4HB), while the T_g of PBAT decreased with increasing content of P(3,4HB).

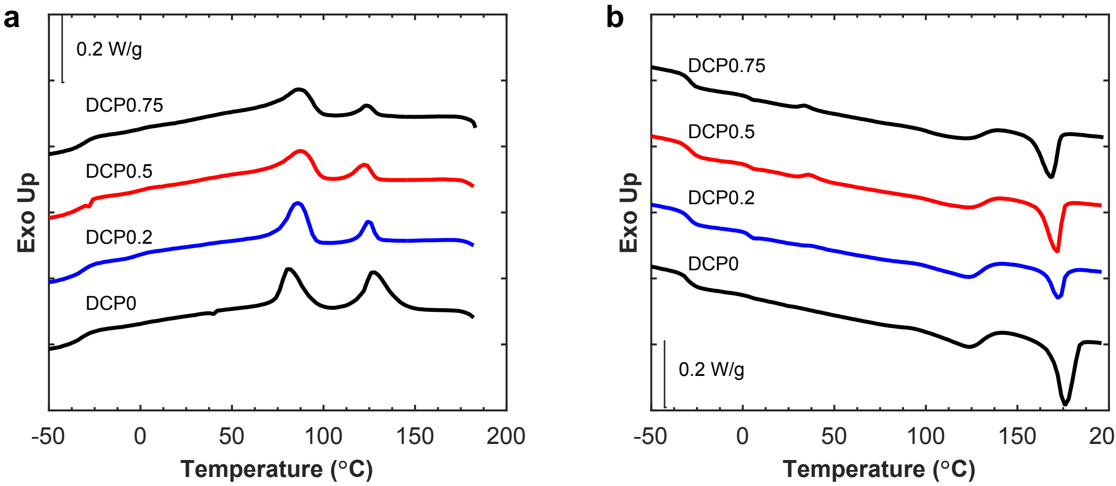

Figure S11: DSC traces of P(3HB):PBAT 20:80 blends with different contents of DCP added, (a) cooling and (b) second heating scans.

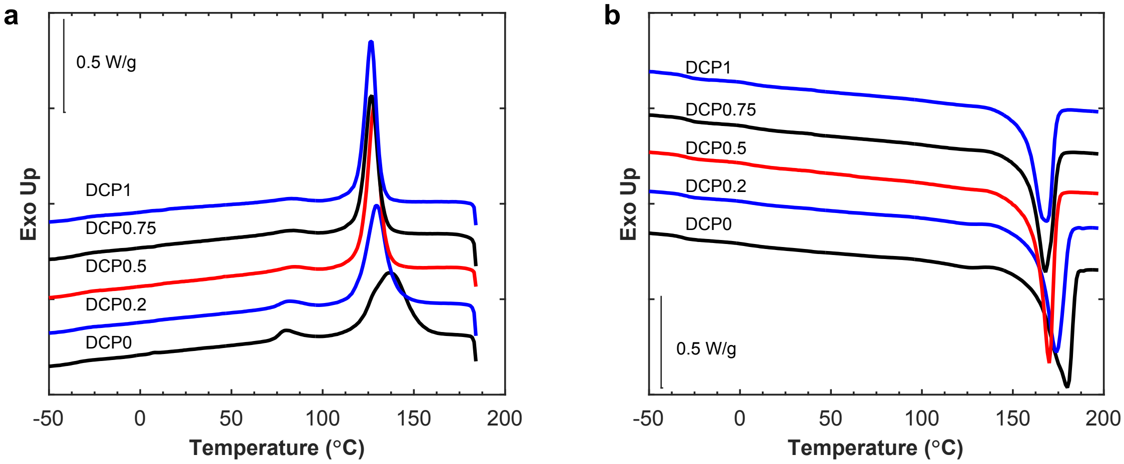

Figure S12: DSC traces of P(3HB):PBAT 60:40 blends with different contents of DCP added: (a) cooling and b) second heating scans at 10 °C/min. There was no visible trend in the T_g value, and the transition was difficult to detect at this heating rate. The crystallinity of the polymers was difficult to determine because of overlapping melting peaks. Still, a small decrease in crystallinity at the addition of 1 wt% DCP was visible from the heating scan. In addition, there was a trend of decreasing melting and crystallization temperatures with the addition of DCP.

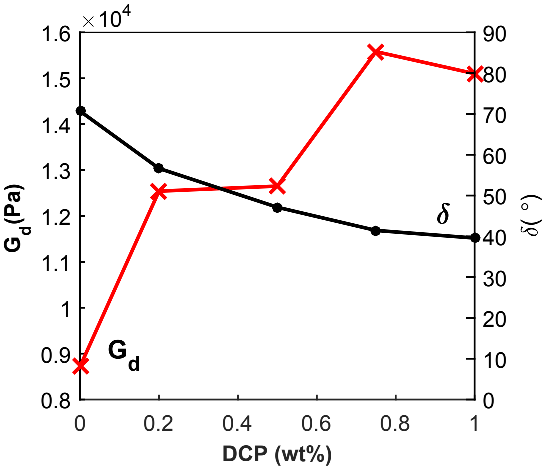

Figure S13: Dynamic shear modulus and phase shift for P(3HB)/PBAT 60:40 blends with different contents of DCP added, as measured by rheology at 1 Hz and 160 °C. The modulus increased with increasing DCP content. In addition, the phase shift decreased with the addition of the peroxide.

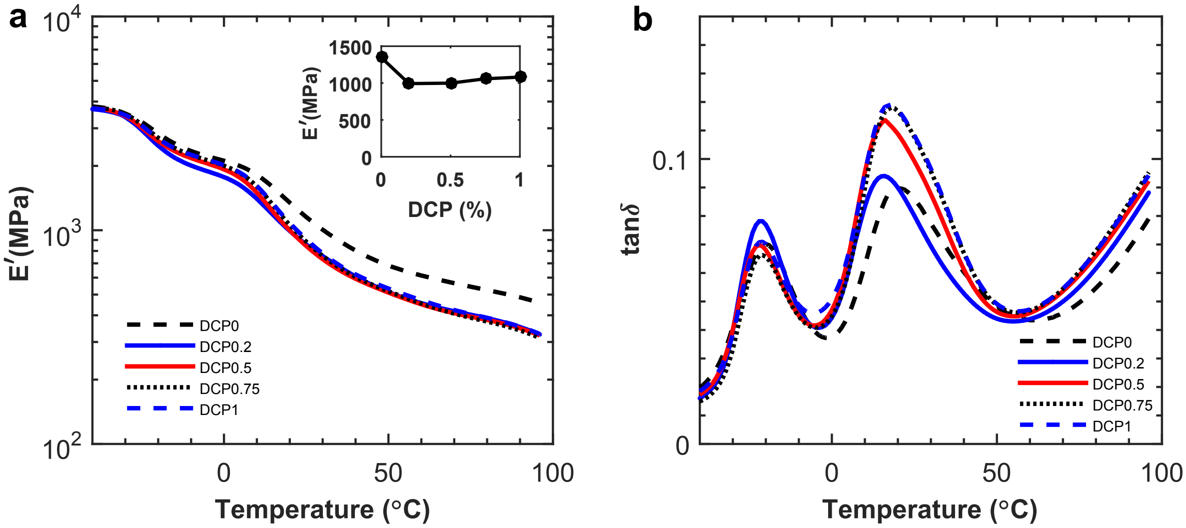

Figure S14: Tensile storage modulus (a) and tan δ curves (b) for P(3HB):PBAT 60:40 blends with different contents of DCP added, analyzed at 3 °C/min and 1 Hz in the linear viscoelastic region: (a) storage modulus and (b) tan δ. The addition of DCP caused a decrease in the modulus at high temperatures, while the amount of added DCP had no effect. At low temperatures there was a decrease in modulus from 0 to 0.2 wt% DCP and then an increasing modulus with increasing amount DCP was observed. The damping ability of P(3HB) increased with the addition of peroxide, as seen in the tan δ data. This may be due to crosslinking of the P(3HB) which formed a gel or due to morphology changes caused by the compatibilization.

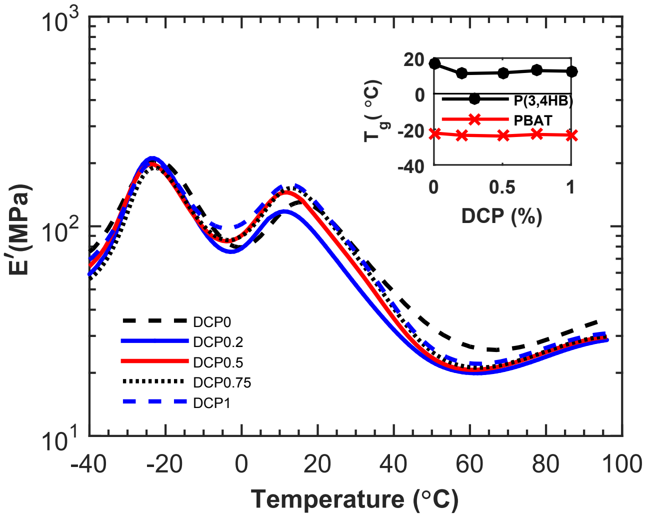

Figure S15: Loss modulus for P(3HB):PBAT 60:40 blends with different amounts of DCP added. The inset shows the T_g for P(3HB) and PBAT. The T_g of P(3HB), as detected from the loss modulus, decreased with the addition of peroxide. There was a small increase in T_g with increasing DCP content when using the level at 0.2 wt% as a reference.